Modeling and Measurement of Toroidal Currents in the HSX Stellarator

J. C. Schmitt[*], **J. N. Talmadge,** and **J. Lore**

HSX Plasma Laboratory, UW-Madison, Madison, WI 53706-1691

A set of magnetic diagnostics, including Rogowski coils, diamagnetic loops and two poloidal 'belts' of 3-axis pick-up coils measure the magnetic field at several locations around HSX. The two belts are separated by $\approx 1/3$ of a field period and measure the local magnetic field vector at 16 poloidal locations at the two toroidal angles. With the VMEC [1] and PENTA [2] codes, a calculation of the Pfirsch-Schlüter (PS) and bootstrap currents is performed. The 3-D equilibrium reconstruction code V3FIT [3] is then used to calculate the expected response of the magnetic diagnostics. The sensitivity of the diagnostic set to features in both the PS and bootstrap current is explored. Because of the lack of toroidal curvature, the dipole PS current has a helical rotation and nearly reverses at the two toroidal locations. The bootstrap current in HSX is in the opposite direction compared to that in a tokamak. Compared to a tokamak, the relative magnitude of each current is reduced by a factor of the effective transform (≈ 3) [4]. The PS current reaches steady state quickly, whereas the bootstrap current rises throughout the discharge on a 50-500 ms timescale. In most cases, the toroidal current is still rising at the end of the discharge, reaching 0.4-0.6 kA. A 3-D model that relies on the calculation of the susceptance matrix [5] is used to calculate the time evolution of the toroidal current.

1 HSX Overview and Diagnostic Set

The Helically Symmetric eXperiment [6] (HSX) is a 4-field period quasihelically-symmetric (QHS) stellarator that has a direction of symmetry in $|B|$. In HSX, $|B| \approx B_0[1 - \epsilon_h cos((n - m\iota)\phi)]$, with toroidal angle, ϕ, $(n, m) = (4, 1)$ and rotational transform, ι. This has some interesting consequences for the toroidal currents. The Pfirsch-Schlüter current rotates with the $|B|$ contours, demonstrating the effective minimization of the toroidal curvature term $(n, m) = (0, 1)$. The reversal and reduction of the bootstrap current, relative to those in a tokamak, are properties of the quasihelical symmetry and high effective transform [4]. The bootstrap current reduces the rotational transform (≈ 1) but increases the effective transform (≈ 3). The decay time of the toroidal current profile is as long or longer than the length of the plasma shot duration, $\tau_{\eta_{||}/\mu_0} \geq \tau_{Exp}$=50 ms.

The results presented here are restricted to the 1 Tesla QHS field configuration. The only source of heating is 1st-harmonic O-mode electron cyclotron resonance heating (ECRH). The microwaves are launched perpendicular to the magnetic axis and little to no current drive has been observed during the 1 Tesla campaign. The same total toroidal current is measured for cases with the main field direction reversed, indicating no toroidal current drive from misaligned ECRH. The electron temperature and density profiles, $T_e(\rho)$ and $n_e(\rho)$, shown in Fig.1a, are measured with the Thomson Scattering system and $T_i(\rho)$ is estimated from impurity radiation with a ChERS system. Passive spectroscopic measurements of the Bremsstrahlung radiation provide the estimate of $Z_{eff} \approx 1$ for most of the plasma profile. Here, the normalized radius is $\rho \equiv \sqrt{\Phi/\Phi_a}$ with Φ defined as toroidal flux enclosed by a flux surface and Φ_a is the toroidal flux enclosed by the last closed flux surface.

The magnetic diagnostic set includes two Rogowski coils, two flux loops and 32 dB/dt sensors. One of the Rogowski coils and the 32 sensors are mounted on the exterior side of the type 304 1/4 inch stainless steel vacuum vessel. The 'skin time' of the vessel is 0.22 ms, so the eddy currents in the vessel are expected to be short lived. Diagnostic ports near the sensors have a similar skin time, or shorter. A sketch of the position of each sensor is indicated by their Poloidal Index in Fig. 2. These diagnostics measure changes in the local magnetic field vector

* Corresponding author: E-mail: jcschmitt@wisc.edu

in their own local orthogonal coordinate system, with the radial direction (B_r) outward normal to the vacuum vessel, and a poloidal direction (B_θ) tangent to the vessel, along the path of the nylon belt upon which the sensors are mounted. The V3FIT code is used to predict the signals at each these diagnostics. The input to this code is a standard VMEC input file that specifies the plasma pressure and current profiles, and a set of specifications for the location, orientation, and type of each diagnostic.
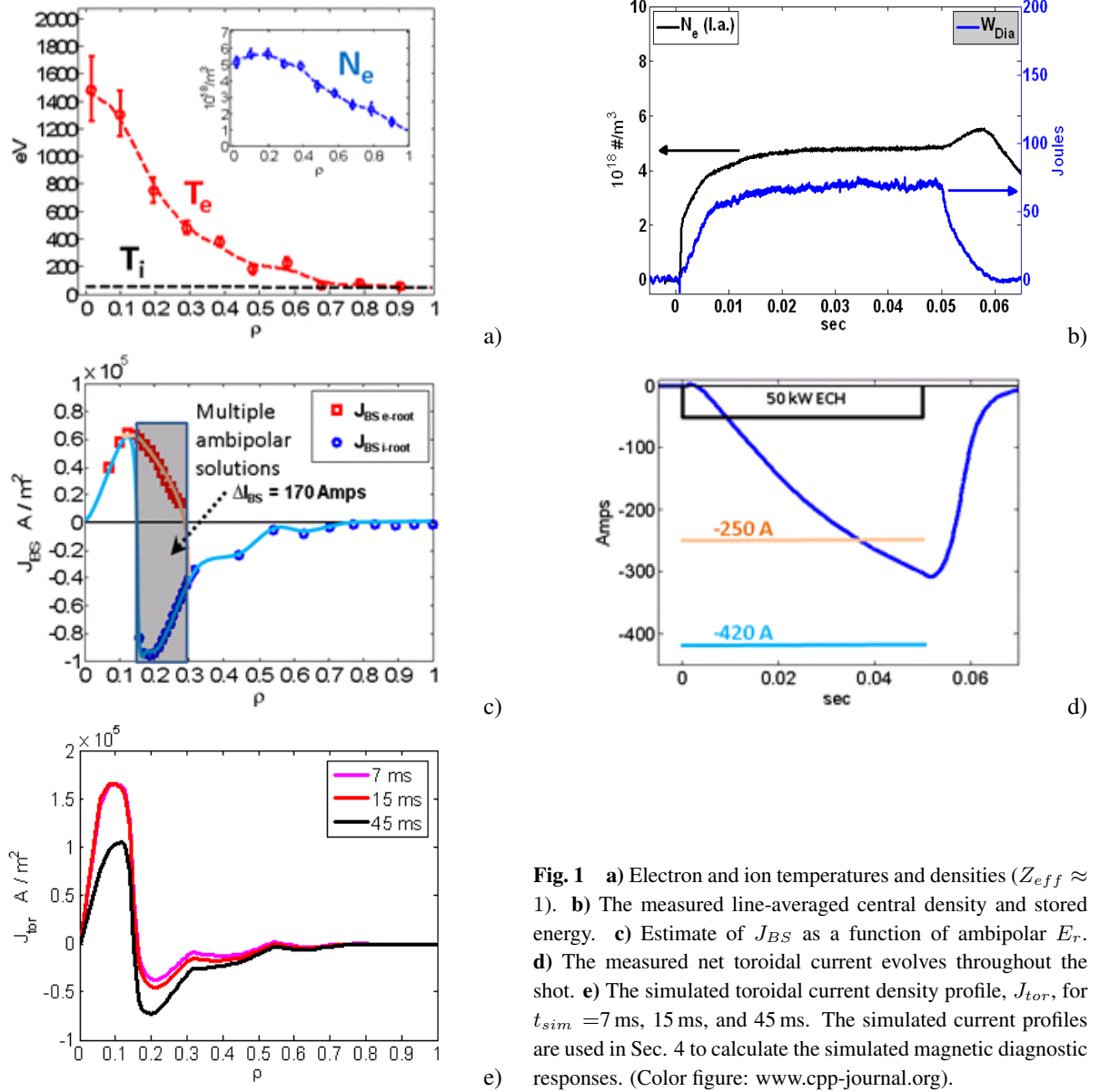

a)

b)

c)

d)

e)

Fig. 1 **a)** Electron and ion temperatures and densities ($Z_{eff} \approx$ 1). **b)** The measured line-averaged central density and stored energy. **c)** Estimate of J_{BS} as a function of ambipolar E_r. **d)** The measured net toroidal current evolves throughout the shot. **e)** The simulated toroidal current density profile, J_{tor}, for $t_{sim} =$7 ms, 15 ms, and 45 ms. The simulated current profiles are used in Sec. 4 to calculate the simulated magnetic diagnostic responses. (Color figure: www.cpp-journal.org).

2 Time Evolution of Toroidal Current Profile

The evolving current profile is modeled with a 1D diffusion equation using a 3D susceptance matrix [5]. This evolution equation is used to simulate the current profile evolution and magnetic diagnostic responses (Sec. 4). The diffusion equation and boundary conditions are:

$$\frac{d\iota}{dt} = \frac{1}{\Phi_a^2} \frac{d}{ds} \left(\eta_{||} V' \left[\frac{\langle B^2 \rangle}{\mu_0} \frac{d}{ds} (S_{11}\iota + S_{12}) + p'(S_{11}\iota + S_{12}) - \langle J_{NI} \cdot B \rangle \right] \right)$$

$$\left. \frac{d\iota}{ds} \right|_{s=0} = 0 \qquad and \qquad \iota_{s=1} = \left(\frac{\mu_0 I(s)}{S_{11}\Phi'} - \frac{S_{12}}{S_{11}} \right)_{s=1}$$

The variables p and V are the plasma pressure and enclosed volume, and the $(')$ are radial derivatives with respect to the radial coordinate, $s \equiv \rho^2$. The current source, J_{NI}, is any non-inductive source (bootstrap, NBI, etc.), and the parallel conductivity, $\eta_{||}$, includes corrections for trapped-particle effects. $I(s)_{s=1}$ is the total toroidal plasma current linked by the Rogowski coil and provides one of the boundary conditions for the diffusion equation. The susceptance matrix quantities, S_{ab}, are flux-surface averages of the metric tensor components. An important observation is to note that for a typical tokamak, $S_{12} = S_{21} = 0$, while for HSX, $-S_{11} \approx S_{12} \approx S_{21}$. Numerical simulations show that this results in a slightly shorter decay time for transient current profiles in HSX, relative to a similar tokamak. The values of the susceptance matrix used throughout this paper are based on the vacuum magnetic configuration. A self-consistent estimate of the bootstrap current density profile and susceptance matrix are beyond the scope of this present work.

The enclosed toroidal current profile, $I(s)$, is related to a toroidal current density profile, J_{tor}, and the rotational transform profile, $\iota(s)$, through the following relations:

$$J_{tor}(s) = \frac{\sqrt{\langle B^2 \rangle}}{\Phi_a} \frac{dI}{ds} \qquad and \qquad \iota(s) = \frac{\mu_0 I(s)}{S_{11}\Phi'} - \frac{S_{12}}{S_{11}}$$

3 Neoclassical Estimate of the Bootstrap Current

The electron temperature and density profiles for a set of similar plasma discharges are shown in Fig.1a. Each plasma realization in this set has a similar measured line-averaged central density and stored energy throughout the shot. The energy confinement time is ≈ 4 ms, based on diamagnetic loop measurements. An example of these quantities for a single shot from this set are shown in Fig.1b. The ECRH location is the same for each of these shots, as is the radiated power (not shown). The steady-state bootstrap current profile, J_{BS}, for the profiles in Fig.1a is modeled by PENTA, assuming a single ion-species with $Z_{eff} = 1$. This estimate is shown in Fig.1c. For $\rho \geq 0.3$, only the 'ion-root' solution for E_r is predicted. In contrast, $\rho \leq 0.15$, there is only the 'electron-root' solution. The region $0.15 \leq \rho \leq 0.3$ has multiple stable ambipolar solutions for E_r. The electron-root reverses the direction of the bootstrap current, compared to that in the ion-root. If the radial electric field was at the electron-root for $\rho \leq 0.3$, the net bootstrap current would be -250 A. In contrast, if the electric field was at the ion-root for $\rho \geq 0.1$, the net bootstrap current would be -420 A.

The ensemble-average of the measured net toroidal current for the same set of shots is shown in Fig.1d. The high electrical conductivity of the plasma results in an effective L/R time that is as long or longer than the length of the plasma shot. Based on the measurements, most of the plasma discharges in this magnetic configuration have L/R times in the range of 50 ms-500 ms. For this particular operating configuration (1T QHS, 50 kW ECRH, maximum central T_e), the measured net current at the end of the ECH time is between the extreme limits of the ion- and electron-root solutions. An estimate of the total steady state current, I_∞, can be extrapolated by fitting the measurement to a decaying exponential model:

$$I(t, s = 1) = I_\infty \left(1 - exp \left(-\frac{t - t_{Breakdown}}{\tau_{L/R}} \right) \right)$$

$\tau_{L/R}$ is the experimental L/R decay time and $t_{Breakdown}$ is the time required to achieve stable plasma conditions and is related to the energy confinement time. For the current evolution in Fig.1d, $t_{Breakdown} \approx 3$ ms - 5 ms, $\tau_{L/R} \approx 40$ ms - 60 ms and $I_{SteadyState} \approx -420A - -500A$. This estimate of the total current is in the range expected for the current profile dominated by the ion-root solution. To estimate the bootstrap current for a tokamak with the same major and minor radii and rotational transform as HSX, the BOOTSJ [7] code was used. The net bootstrap current for this "equivalent tokamak" is +2040 A, which is much larger and opposite to that measured in HSX. The effects of QHS and high effective transform are the reversal and reduction of the bootstrap current, respectively.

4   Helical Rotation of the Pfirsch-Schlüter Current and Profile Evolution

The magnetic diagnostics are sensitive to the magnetic fields generated by the Pfirsch-Schlüter, bootstrap, inductive, and (to a lesser extent) diamagnetic currents. A forward-prediction model ($t_{sim} = 0$ to 50 ms) of the evolving current profile (Sec. 2), combined with the pressure profile, is used as input for V3FIT (which uses VMEC as its equilibrium solver) to predict the signals for each of the magnetic diagnostics present on HSX. For this case, the steady-state current profile is the one that is dominated by the PENTA ion-root solution, Fig. 1b, $I_{BS} = -420A$. The simulated toroidal current density profile, $J_{tor}(\rho)$ is shown in Fig.1e for simulation times of 7 ms, 15 ms and 45 ms.
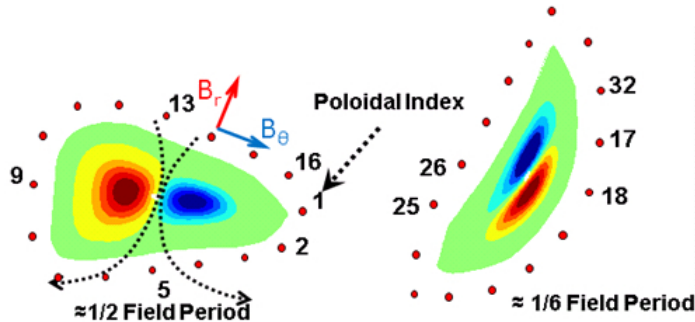

Fig. 2 The 32 dB/dt sensors at two toroidal locations. Each has a unique Poloidal Index. A sketch of J_{PS} at the toroidal locations is shown. The inboard/outboard dipole current density nearly reverses between the two toroidal locations. The 'local' B_r & B_θ directions are shown for the sensor at Poloidal Index=14. (Color figure: www.cpp-journal.org).

The effect of the Pfirsch-Schlüter current is seen by using V3FIT to calculate the field due to the plasma pressure with no net toroidal current, $J_{tor}(s) = 0$ (see Fig. 2 for a sketch of J_{PS}). In Fig. 3, the expected signal strength for the local radial and poloidal signals at each diagnostic is plotted (dotted lines). A dipole-like response can be seen in the pattern. The sign of the simulated signals at the two toroidal locations have a phase shift in their Poloidal Index, demonstrating the helical rotation of the Pfirsch-Schlüter current between these two locations. The expected signals @ t_{sim}=7 ms are shown (dashed lines). The net current is small (30 A) and contributes a noticeable shift in the B_θ signal for all diagnostics. The diagnostic signals from the shot-by-shot ensemble average, averaged over a window 3 ms $< t_{Exp} <$7 ms are also shown. They agree well in terms of sign and phase. There is also reasonable agreement in the magnitude of the signals.
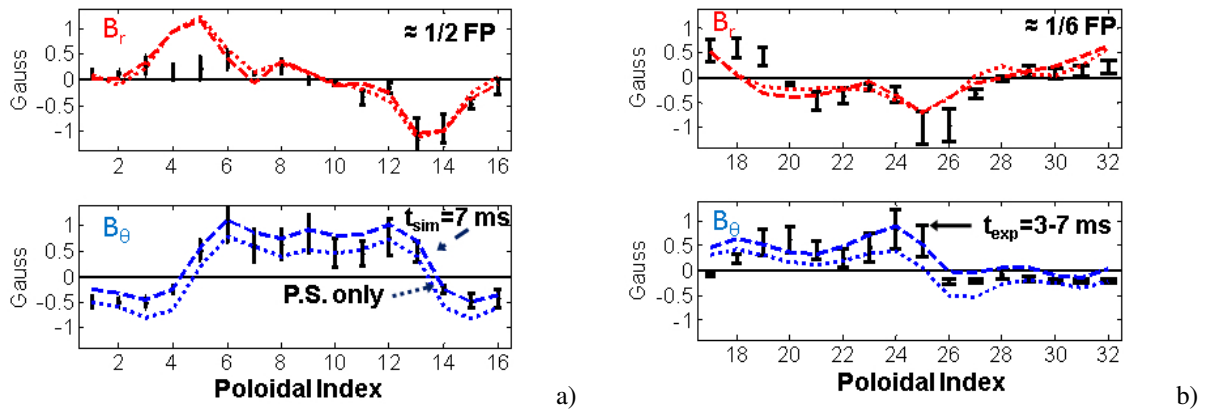

Fig. 3 The magnetic field components, B_r and B_θ, in the local coordinate system of the sensor, as a function of Poloidal Index for positions **a)** ≈1/2 Field Period and **b)** ≈1/6 Field Period. (Color figure: www.cpp-journal.org).

The magnetic signals for experimental and simulated times, t_{exp} = 15 ms, 45 ms and $t_{sim} = 15\,ms, 45\,ms, \infty$, are shown in Fig. 4 (red, black points and red-dashed, black-dashed, blue-dotted lines). The last case is equivalent to the steady state bootstrap current. The bootstrap current becomes the largest measurable plasma effect, both simulated and measured, for the later times. The poloidal field component, B_θ, demonstrates the effect of the net toroidal current on the field around the plasma column. The shape of the vacuum vessel, with respect to the field normal to the vacuum vessel, produces an m=2 structure in the B_r signal.

There is good agreement in comparison of the measured and modeled magnetic field components. The sign and phase of the signals agree across the majority of the diagnostic array. However, the measured profiles appear to reach their equilibrium level at a rate somewhat faster than predicted by the model, and at least one subset of sensors (17-21) shows unexplained trends. Alignment of the sensors, the estimate of Z_{eff}, the initial plasma profiles, and the neoclassical calculation of the bootstrap current are all possible sources of error. Current in the vacuum vessel is not routinely measured, but experiments at 1/2 Tesla have shown the toroidal current in the vacuum vessel is, at most, a few amps, and its effect on the diagnostic signals is neglected at this point. Other differences may be resolved by an equilibrium reconstruction with V3FIT.
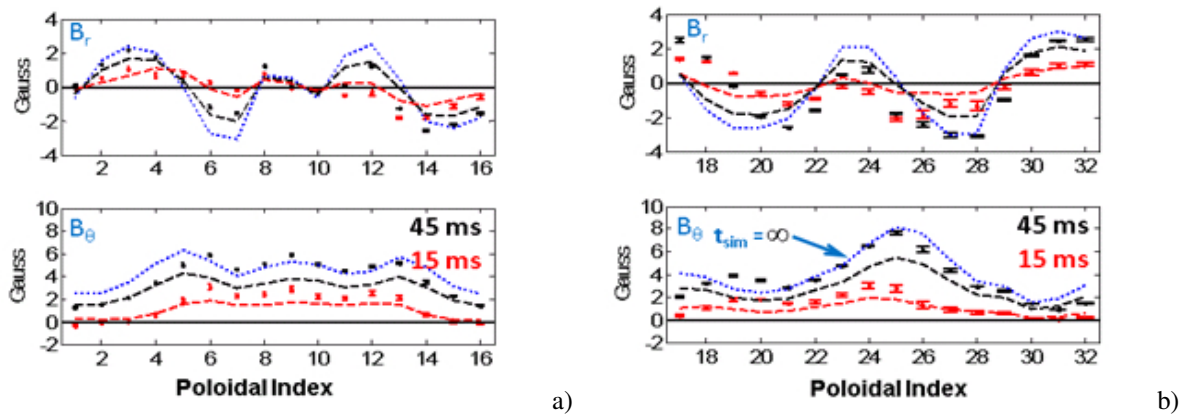

Fig. 4 B_r and B_θ for the toroidal locations in Fig. 2. t_{Exp} = 15 ms (red points), t_{Exp}=45 ms (black points), t_{sim} = 15 ms (red-dashed lines), t_{sim} = 45 ms (black-dashed lines), and $t_{sim} = \infty$ (blue-dotted lines). (Color figure: www.cpp-journal.org).

5   Conclusions and Next Steps

In the HSX, the effect of quasihelical symmetry on the toroidal currents has been studied. The effective removal of the toroidal curvature is demonstrated by measuring the helical rotation of the Pfirsch-Schlüter current with the $|B|$ contours. The high effective transform and quasihelical symmetry are demonstrated by the reduction and reversal of the bootstrap current, compared to a tokamak. The evolving current profile is modeled with a 1D diffusion equation using a 3D susceptance matrix. PENTA provides the estimate of the bootstrap current profile. The V3FIT code calculates the expected signal response for an array of magnetic diagnostics installed on HSX. The evidence of the Pfirsch-Schlüter current is seen early in the plasma discharge, before the effect of the bootstrap-driven currents become large. Later in the shot, the bootstrap-driven currents dominate the Pfirsch-Schlüter currents, in terms of signal contribution at the sensors. Comparing the measured and modeled signals, the sign and phase of the the signals agree well. The next step will be to use V3FIT for equilibrium reconstruction of HSX plasmas.

References

[1] S.P. Hirshman and J.C. Whitson, Phys. Fluids **26**, 3553 (1983).
[2] D.A. Spong, Phys. Plasmas **12**, 056114 (2005).
[3] J.D. Hanson, et al., Nucl. Fusion **49**, 075031 (2009).
[4] J.N. Talmadge, V. Sakaguchi, F.S.B. Anderson, D.T. Anderson, and A.F. Almagri, Phys. Plasmas **8**, 5165 (2001)
[5] P.I. Strand and W.A. Houlberg, Phys. Plasmas **8**, 2782 (2001).
[6] F.S.B. Anderson, et al., Fusion Technol. **27**, 273 (1995).
[7] K.C. Shaing, et al., Phys. Fluids B **1**, 1663 (1989).